Journal of Materials Chemistry C

Accepted Manuscript

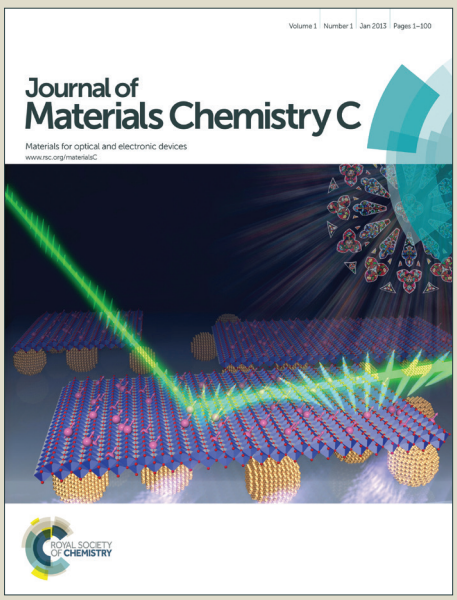

ROYAL SOCIETY OF CHEMISTRY

www.rsc.org/materialsC

Graphical Abstract

Decreasing reflection through the mutually positive effects of nanograss and nanopillars

C. H. Lin,[a,b] J. Shieh,*[c] C. C. Liang,[a] C. C. Cheng[d] and Y. C. Chen[e]

[a] Department of Photonics, National Cheng Kung University, Tainan, Taiwan.

[b] Advanced Optoelectronic Technology Center, National Cheng Kung University, Tainan, Taiwan.

[c] Department of Materials Science and Engineering, National United University, Miaoli, Taiwan. E-mail: jshieh@nuu.edu.tw

[d] Department of Physics, National Central University, Taoyuan, Taiwan.

[e] Department of Electrical Engineering, Chung Hua University, Hsinchu, Taiwan.

A combination of a nanograss and a nanopillar array provides mutually enhanced antireflection performance.

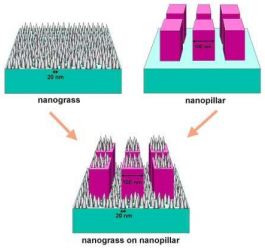

Journal of Materials Chemistry C

RSCPublishing

ARTICLE

Decreasing reflection through the mutually positive effects of nanograss and nanopillars

Cite this: DOI: 10.1039/xoxxoooooox

C. H. Lin,[a,b] J. Shieh,*[c] C. C. Liang,[a] C. C. Cheng[d] and Y. C. Chen[e]

Received,
Accepted

DOI: 10.1039/xoxxoooooox

www.rsc.org/

Although individual biomimetic nanograss and nanopillar arrays have been investigated widely to decrease surface reflections in energy applications, there have been few studies using them in combination to improve antireflection properties. Using hydrogen plasma to fabricate a silicon nanograss on a nanopillar array, we could decrease the reflection of the nanograss at longer wavelengths, while decreasing the non-specular reflection of the nanopillars over a wide spectral range. Simulations based on rigorous coupled-wave analysis supported the experimental data.

Introduction

Antireflective surfaces are essential in many applications, including solar cells[1–3] and light-emitting diodes.[4,5] Coating a thin film onto a substrate is a conventional means of minimizing reflection through destructive interference of light waves reflected from the air–coating and coating–substrate interfaces. This approach can be harnessed, however, only at a specific wavelength, depending on the coating's refractive index and thickness.[6] Because reflection arises from a change in refractive index at the interface between two media, biomimetic moth-eye nanostructures featuring graded refractive index profiles have been suggested to mitigate the refractive index change and provide broadband antireflection characteristics.[7–9] The diameter of such a moth-eye structure should be much less than the incident wavelength[10] to avoid diffused scattering from increasing the total reflectance.[11] In addition, the height of the nanostructure must be sufficiently large for the light to "see" the graded profile. Accordingly, the optimal profile of an antireflection moth-eye structure would be characterized by a small diameter and a high depth-to-diameter aspect ratio. Unfortunately, features having a submicron diameter and a high aspect ratio have the problem of mechanically instability; in addition, when applied in photovoltaic devices, a high-aspect-ratio profile has the drawback of higher carrier recombination on the surface area.[12–14] The use of a material having a higher absorption coefficient can decrease the required aspect ratio by shortening the absorption length. For example, we have demonstrated that the application of high-absorption amorphous silicon (*a*-Si) can provide an average total reflectance of 0.34% from a thin (<680 nm) *a*-Si/Si double layer.[15]

Despite some problems relating to mechanical stability and surface defects, the preparation of high-aspect-ratio profiles of nanopillars and nanowires continues to attract much attention for the development of nanostructured solar cells. With their shorter minor-carrier diffusion lengths, the purity requirements of Si nanowire/nanopillar solar cells can be lower than those of traditional cells, thereby decreasing production costs.[16–20] In a radial-junction nanowire/nanopillar array solar cell, the diameter should be on the order of the minority-carrier diffusion length to ensure efficient carrier collection.[21] The diffusion length of the minority carrier depends on the quality of the materials used; it can range from hundreds of nanometers to several micrometers.[22] For example, the diffusion length in single-crystal silicon is typically much greater than 100 nm; improved carrier collection will, therefore, require the diameter of the nanorod to be greater than a quarter of the wavelength of visible light, thereby possibly diffracting the incident light to decrease the degree of light absorption. As a result, challenges remain in optimizing the aspect ratio, periodicity, and size of the protuberances when developing nanostructured solar cells.

An alternative approach toward improving the absorption of nanowires or nanopillars is the use of multilevel hierarchical structures, usually integrating micro- and nanostructures together.[23–28] With a sufficient number of nanostructural levels, the absorption of a multi-diameter nanopillar should reach close to that of a moth-eye-like nanocone.[29] The investigation of multilayer nanostructures is, however, cumbersome because of the difficulty in fabricating one nanostructure on top of another over a large area.[30] Here, we report a two-level nanostructure that combines a 20-nm–diameter nanograss as the top layer and 100-nm–diameter nanopillars as the bottom layer. To support our experimental results, we have also performed simulations through rigorous coupled-wave analysis (RCWA). With this nanostructure, exhibiting double roughness, we reveal that the antireflection properties of a nanopillar array can be improved by the presence of tinier nanostructures on its surface, and that the reflection of an array of moth-eye structures can be decreased by the presence of another nanostructure beneath it. That is, in this two-layer nano-on-nano structure, the antireflection properties of the nanograss and the nanopillars were each improved by the presence of the other.

Experimental

The silicon nanograss was prepared through inductively coupled plasma chemical vapor deposition (ICPCVD) with hydrogen plasma as an etching species.[31,32] CF_4 and O_2 plasma were used to clean the chamber prior to hydrogen plasma etching. The base pressure was 5×10^{-5} torr; the substrate

holder was heated at 400 ℃. Hydrogen gas (feeding rate: 160 sccm) was used to etch a 6-inch (100) Si wafer at a reactor pressure of 30 mtorr. The 13.56-MHz RF power and the 300-kHz bias power were set at 550 and 280 W, respectively. The nanopillar patterns were fabricated using electron beam lithography (Leica WEPRINT 200) and a transformer-coupled plasma system (Lam TCP 9400) to give an average pillar height of approximately 1 μm. The process of creating the two-layer nano-on-nano structure involved fabricating the nanopillar array first and then using it as the substrate for the deposition of the nanograss. The morphologies of the nanostructures were characterized using scanning electron microscopy (JEOL JSM 6500F). Optical spectra were recorded in the range 220–1000 nm at room temperature using a Jasco V-670 spectrometer (for specular reflectance) and a Hitachi U-4100 spectrometer with an integrating sphere (for total reflectance).

Results and discussion

To prepare the nanopillar array, we performed electron beam lithography in conjunction with a plasma dry etching process. We used inductively coupled hydrogen plasma without a lithographic mask to create the nanograss on the surface of the nanopillars.[31,32] Scanning electron microscopy (SEM) images of the nanopillars before and after hydrogen plasma etching revealed that the nanograss was distributed uniformly throughout the surface profile of the nanopillars, thereby constituting a double-layer Si nanostructure (Figure 1). The base diameter and blade length of the features in the nanograss were 20 and 290 nm, respectively; the nanopillars were characterized by a diameter of 100 nm and a spacing of 200 nm.

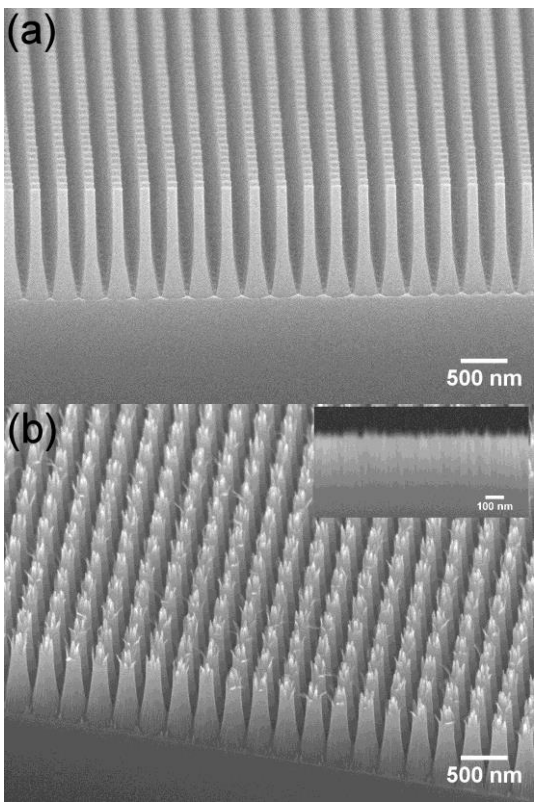

Fig. 1. Tilt-view SEM images of (a) single-layer nanopillar and (b) double-layer nanograss-on-nanopillar nanostructures. Inset: Cross-sectional SEM image of the nanograss.

Figure 2 displays the specular and total reflectance of the nanograss; the reflectance spectrum of a silicon wafer is also presented for comparison. The reflectance of the silicon wafer from 220 to 1000 nm was greater than 31%, with peaks at 272 and 364 nm related to the interband transition.[33] With its gradual decrease in effective refractive index away from the surface (i.e., the sharp difference in refractive index between the air and the silicon wafer was smoothed out), the nanograss dramatically suppressed the reflection of the silicon wafer (<5% from 220 to 1000 nm). In addition, because we fabricated the nanograss without an additional mask, the length of each blade of nanograss was approximately the same; hence, we could neglect any scattering from the rough air–nanograss interface. Notably, the difference between the specular and total reflectance was also insignificant in Figure 2, revealing that no high-order diffraction arose from the subwavelength nanograss, thereby inhibiting the nonspecular reflectance. The increase in reflectance at larger wavelength arose from the interface between the air and the silicon wafer appearing relatively sharp when the wavelength of the light was greater than several times of the height of the nanograss.[10] The thin nanograss layer was not evident to longer wavelengths of light; therefore, the incident light was reflected partially from the interface between the nanograss and the bulk silicon underlayer.

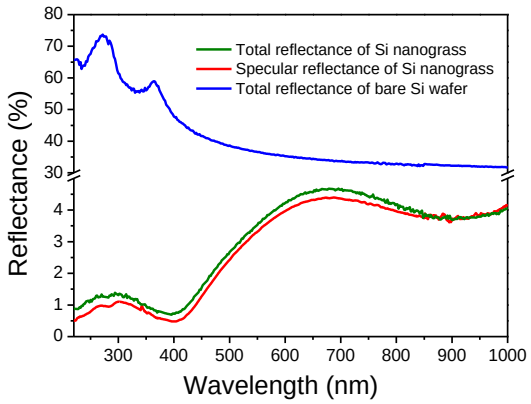

Fig. 2. Specular and total reflectance from the nanograss structure and total reflection from a Si wafer.

To decrease the reflectance of the nanograss toward light at longer wavelengths, we fabricated a nanopillar array to replace the flat silicon as the underlayer for the nanograss. Figure 3a presents the specular and total reflectance spectra of the nanopillar array, in which the reflectance oscillated with respect to the wavelength. A three-dimensional numerical simulation based on RCWA revealed that this oscillation in a nanopillar array is similar to the behavior of a thin film.[7] Notably, although our nanopillars had small diameters (100 nm), smaller than those that can be created using most top-down nanofabrication approaches, differences remained between the specular and total reflectance spectra. The diffused reflectance increased as the incident wavelength decreased. The specular reflectance was less than 3.6% whereas the total reflectance increased up to the 10% level, especially at the peak of the interband transition, revealing that high-order reflection cannot be ignored when the period of the nanopillars was less than the wavelength of the illuminating light. The incident light illuminated the sample center with a beam size less than the area of the nanopillar array (1×1 cm^2). The port size of the integrating sphere was, however, larger than the area of the nanopillar array. The scattered light that reflected from the non-

patterned part of the sample may have contributed to the total reflection. After adopting this nanopillar array as an underlayer for the nanograss, the reflectance of both the nanograss and the nanopillars changed dramatically: the specular reflectance decreased to less than 1% and the total reflectance decreased to less than 2.5% in the range 220–1000 nm (Figure 3b). A smaller difference between the specular and total reflectance remained, revealing that the light that passed through the nanograss layer further penetrated into the nanopillar array and was diffracted by the pillar pattern. Notably, the reflectance of the nanopillar array was suppressed by the presence of the tinier nanofeatures on its surface—without varying the diameter, aspect ratio, or spacing of the nanopillars.

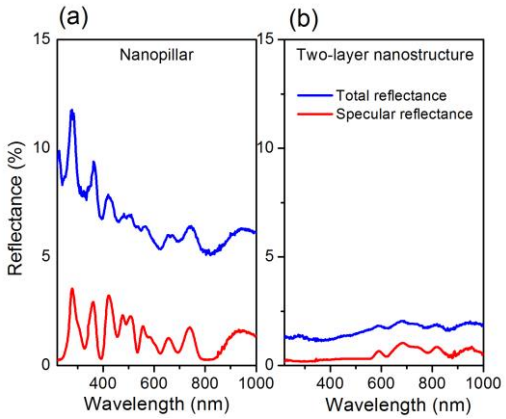

Fig. 3. Specular and total reflectance from (a) single-layer nanopillar and (b) double-layer nanograss-on-nanopillar nanostructures.

Figure 4 displays specular reflectance measurements for both TE- and TM-polarized light on both the single-layer nanopillar and double-layer nanograss-on-nanopillar nanostructures at incident angles varying from 20 to 60°. The two-layer nanostructure provided superior antireflection properties over broad wavelengths and wide angles of incident light, implying that it has great potential for use in solar cell devices exhibiting higher photoelectric conversion efficiencies as a result of lower surface reflection.

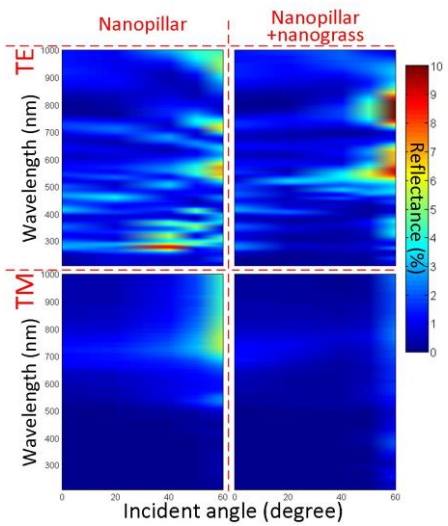

Fig. 4. Specular TE and TM reflectances for single-layer nanopillar and double-layer nanograss-on-nanopillar nanostructures, measured at various incident angles and wavelengths.

To further explore the antireflective behavior of the two-layer nanostructure, we performed simulations using an RCWA code developed in-house.[34] Figure 5a provides a schematic representation of the geometry of the simulated structures. Each simulated nanopillar comprised an upper cylindrical rod and a lower truncated cone–shaped structure to mimic the fabricated nanopillar structures in Figure 1a. The simulated nanopillar array featured a rectangular arrangement with a period of 300 nm. The diameter and height of the upper cylindrical rods of the nanopillars were set at 100 and 700 nm, respectively; the base diameter and height of the truncated cones were set at 250 and 500 nm, respectively. These parameters are similar to the dimensions of our fabricated nanopillar arrays. For comparison, we also simulated systems in which the base diameters of the truncated cones were 150 and 200 nm. For simulations of the nanograss, we assumed a nanocone array in a hexagonal arrangement having a period of 22 nm. For the simulated nanograss-on-nanopillar nanostructure, we set the nanograss on top of a base of nanopillars. Any nanograss on the sides of the nanopillars was neglected to simplify the simulation. In all of the following simulations, we set the grass diameter and grass height at 20 and 290 nm, respectively. The nanostructures with taper profiles can be approximated as a stack of lamellar gratings in RCWA.[34,35] We used ten-layer lamellar gratings to approximate the lower truncated cone-shaped structure in a nanopillar and the nanocone structure of a nanograss, as shown in the Supporting Information (Figure S1). Figure 5b presents the simulated reflectance spectra of the single-layer nanopillar and double-layer nanograss-on-nanopillar nanostructures at normal incidence with wavelengths ranging from 200 to 1100 nm. For the nanopillar-only structures, the total reflectance spectrum of the nanopillars having a base diameter 150 nm featured strong interference fringes, with an intensity maximum of up to 20%, that arose from the optical features of the rod-like structures. After introducing tapered structures with greater base diameters (200 or 250 nm), the intensities of the interference fringes in the reflectance spectra decreased significantly. We attribute this phenomenon to the graded index of the antireflective coating approximating the graded index of the nanostructures.[8] The simulated spectrum of the sample with a 250-nm base diameter agreed well with the measured spectrum in Figure 3a. The overlay of the simulated and measured specular reflection is presented in the Supporting Information (Figure S2), which also reveals that the reflectance from the double-layer nanostructure was lower than that from the single-layer nanopillar structure.

The reflectance decreased dramatically for all base diameters after further applying the nanograss on the nanopillar arrays (Figure 5b). For the nanopillar-only structures, we could not readily control the etching parameters to obtain nanostructures with an optimized antireflective graded index. We found, however, that optimization of the nanopillar structures was not crucial for the nanograss-on-nanopillar two-layer nanostructures. Through simple treatment of the nanopillar structures with the nanograss, the reflectance could be decreased dramatically even without optimization of the nanopillar structures. The sharp discontinuity in refractive index between the interface of the nanopillars and the air was further smoothed out after the introduction of the nanograss. To investigate the omnidirectional performance of these nanostructures, we simulated the corresponding total reflectance spectra with incident angles ranging from 0 to 70° (Figure 5c). For the nanopillar-only structure, we simulated an array featuring a base diameter of 250 nm. Even through the

performance of this nanopillar structure was better than that of the arrays having smaller base diameters, it still exhibited high reflectance for light at wavelengths of less than 400 nm, especially at large incident angles. Notably, the optical behavior of the nanograss-only structure was different from that of the nanopillar-only structure. Although its reflectance was higher than that of the nanopillar-only structure at wavelengths greater than 400 nm, it exhibited good antireflective behavior even at larger incident angles for light at wavelengths of less than 400 nm, with reflectance of less than 2% for most of the conditions. After introducing the nanograss onto the nanopillars to form the two-layer nanostructures, the reflectance was suppressed significantly in all wavelength regions. The overlays of measured and simulated results of specular reflections from nanopillars and two-layer nanostructures at oblique illumination for both TE and TM polarizations are presented in the Supporting Information (Figure S3). The nanograss-on-nanopillar two-layer nanostructures behaved as broadband, omnidirectional antireflective coatings. Moreover, we used RCWA to observe the optical behavior of the nanostructures within the near-field regime. Figure 5d displays three-dimensional near-field images of the nanopillar-only structure and the nanograss-on-nanopillar two-layer nanostructure with the illuminating light at normal incidence and the electric field orientated along the *y*-axis. To observe significant differences in the antireflective performance of these two nanostructures, we chose an illuminating wavelength of 250 nm. The presence of the nanograss on the nanopillar arrays allowed the light to penetrate deeper into the nanostructures, increasing the light trapping ability and, thereby, decreasing the reflection of light.

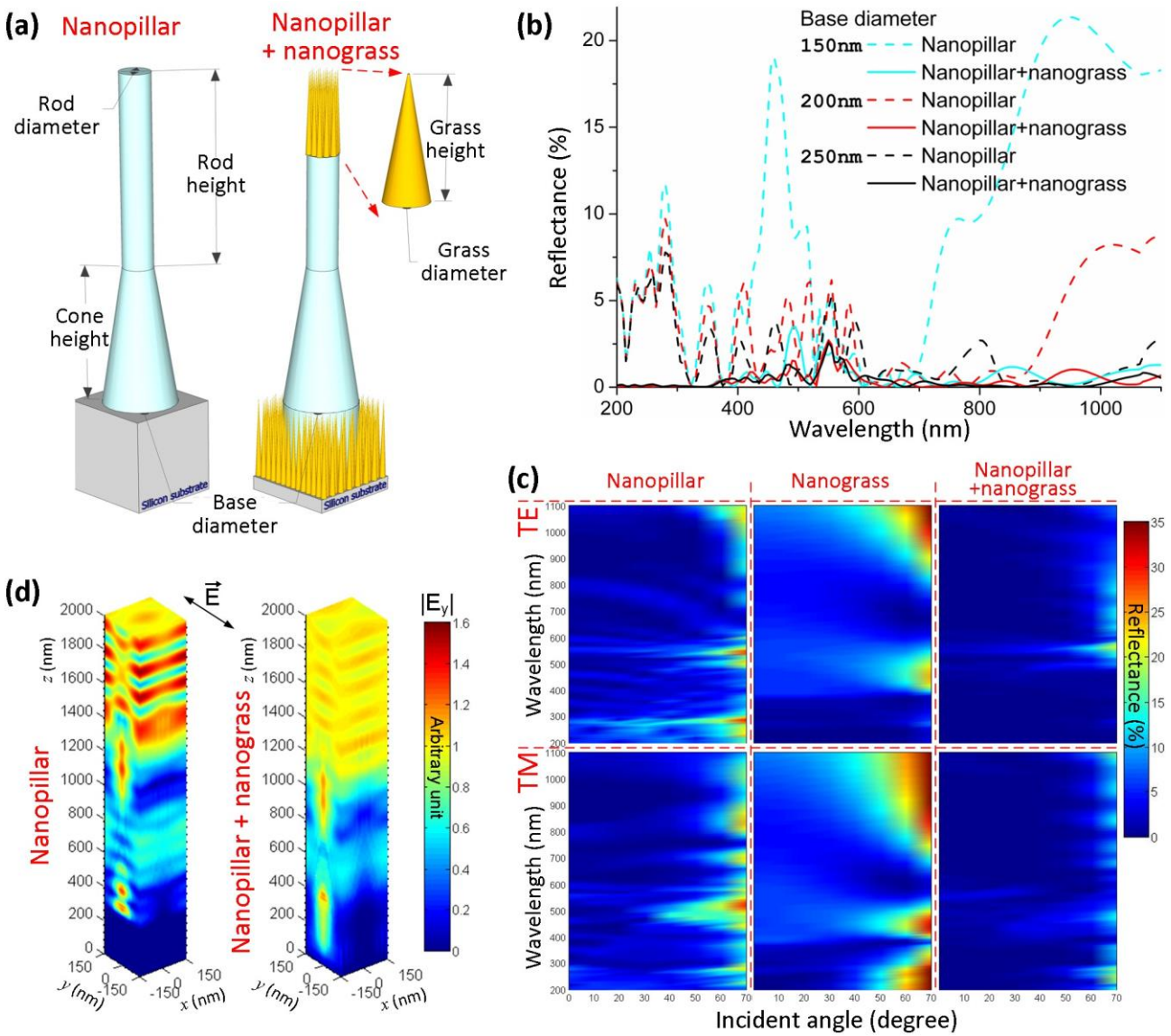

Fig. 5. (a) Schematic representation of the geometries of the simulated structures. (b) Simulated total reflectance spectra of the single-layer nanopillar and double-layer nanograss-on-nanopillar nanostructures; the base diameter of the nanopillars was 150, 200, or 250 nm. (c) Simulated total angular-dependent reflectance of the single-layer nanopillar and nanograss and double-layer nanograss-on-nanopillar nanostructures, with incident angles ranging from 0 to 70°. (d) Three-dimensional near-field images of the nanopillar-only structure and the nanograss-on-nanopillar two-layer nanostructure. All diffraction orders of reflections are included in (a)–(c). The base diameter of the nanopillars in (c) and (d) was 250 nm.

Journal of Materials Chemistry C RSCPublishing

ARTICLE

Conclusions

In summary, we have used a semiconductor-compatible process to develop nanograss-on-nanopillar hierarchal antireflective nanostructures. The tiny dimensions of the nanograss inhibited nonspecular reflectance. Introducing a nanopillar array as an underlayer could minimize the reflectance of the nanograss at higher wavelengths; on the other hand, the reflectance of the nanopillars could be decreased by forming the nanograss on its surface, without changing the geometric parameters of the array. Such materials might be useful in the development of antireflective devices, such as radial junction nanopillar array solar cells.

Acknowledgments

We thank the National Nano Device Laboratories for assistance with nanostructure fabrication; the National Science Council of Taiwan (NSC 99-2221-E-239-043 and NSC 101-2628-E-239-002-MY3) for financial support; F. J. Hou for help with the e-beam lithography; H. M. Chen and C. Y. Ji for recording the SEM images; and S. P. Yang for performing the plasma process.

Notes and references

[a] Department of Photonics, National Cheng Kung University, Tainan, Taiwan.

[b] Advanced Optoelectronic Technology Center, National Cheng Kung University, Tainan, Taiwan.

[c] Department of Materials Science and Engineering, National United University, Miaoli, Taiwan. E-mail: jshieh@nuu.edu.tw

[d] Department of Physics, National Central University, Taoyuan, Taiwan.

[e] Department of Electrical Engineering, Chung Hua University, Hsinchu, Taiwan.

1 E. Garnett, P. Yang, *Nano Lett*., 2010, **10**, 1082.

2 J. Zhu, Z. Yu, G. F. Burkhard, C. M. Hsu, S. T. Connor, Y. Xu, Q. Wang, M. McGehee, S. Fan, Y. Cui, *Nano Lett.*, 2009, **9**, 279.

3 H. M. Branz, V. E. Yost, S. Ward, K. M. Jones, B. To, P. Stradins, *Appl. Phys. Lett.*, 2009, **94**, 231121.

4 H. Kasugai, Y. Miyake, A. Honshio, S. Mishima, T. Kawashima, K. Iida, M. Iwaya, S. Kamiyama, H. Amano, I. Akasaki, H. Kinoshita, H. Shiomi, *Jpn. J. Appl. Phys*., 2005, **44**, 7414.

5 Y. Ou, D. D. Corell, C. Dam-Hansen, P. M. Petersen, H. Ou, *Opt. Exp*., 2011, **19**, A166.

6 S. Walheim, E. Schäffer, J. Mlynek, U. Steiner, *Science*, 1999, **283**, 520.

7 J. Shieh, C. H. Lin, M. C. Yang, *J. Phys. D*, 2007, **40**, 2242.

8 C. T. Wu, C. H. Lin, C. Cheng, C. S. Wu, H. C. Ting, F. C. Chang, F. H. Ko, *Chem. Mater.*, 2010, **22**, 6583.

9 S. Ravipati, J. Shieh, F. H. Ko, C. C. Yu, H. L. Chen, C. T. Wu, S. H. Chen, *Energy Environ. Sci*., 2012, **5**, 7601.

10 S. J. Wilson, M. C. Hutley, *Opt. Acta*, 1982, **29**, 993.

11 H. C. Chang, K. Y. Lai, Y. A. Dai, H. H. Wang, C. A. Lin, J. H. He, *Energy Environ. Sci.*, 2011, **4**, 2863.

12 E. Garnett, P. Yang, *Nano Lett*., 2010, **10**, 1082.

13 J. Li, H. Y. Yu, Y. Li, F. Wang, M. Yang, S. M. Wong, *Appl. Phys. Lett*., 2011, **98**, 021905.

14 B. Dou, R. Jia, H. Li, C. Chen, W. Ding, Y. Meng, Z. Xing, X. Liu, T. Ye, *Appl. Phys. Lett.*, 2012, **101**, 183901.

15 S. Ravipati, J. Shieh, F. H. Ko, C. C. Yu, H. L. Chen, *Adv. Mater*., 2013, **25**, 1724.

16 B. M. Kayes, H. A. Atwater, N. S. Lewis, *J. Appl. Phys*., 2005, **97**, 114302.

17 E. C. Garnett, P. Yang, *J. Am. Chem. Soc.*, 2008, **130**, 9224.

18 K. Q. Peng, S. T. Lee, *Adv. Mater*., 2011, **23**, 198.

19 E. C. Garnett, M. L. Brongersma, Y. Cui, M. D. McGehee, *Annu. Rev. Mater. Res.*, 2011, **41**, 269.

20 R. Yu, Q. Lin, S. F. Leung, Z. Fan, *Nano Energy*, 2012, **1**, 57.

21 M. D. Kelzenberg, S. W. Boettcher, J. A. Petykiewicz, D. B. Turner-Evans, M. C. Putnam, E. L. Warren, J. M. Spurgeon, R. M. Briggs, N. S. Lewis, H. A. Atwater, *Nat. Mater.*, 2010, **9**, 239.

22 A. I. Hochbaum, P. Yang, *Chem. Rev.*, 2010, **110**, 527.

23 H. Xu, N. Lu, G. Shi, D. Qi, B. Yang, H. Li, W. Xu, L. Chi, *Langmuir*, 2011, **27**, 4963.

24 C. H. Chang, P. Yu, M. H. Hsu, P. C. Tseng, W. L. Chang, W. C. Sun, W. C. Hsu, S. H. Hsu, Y. C. Chang, *Nanotechnology*, 2011, **22**, 095201.

25 Y. M. Song, G. C. Park, S. J. Jang, J. H. Ha, J. S. Yu, Y. T. Lee, *Opt. Exp*., 2011, **19**, A157.

26 Y. Xiu, S. Zhang, V. Yelundur, A. Rohatgi, D. W. Hess, C. P. Wong, *Langmuir*, 2008, **24**, 10421.

27 V. Zorba, E. Stratakis, M. Barberoglou, E. Spanakis, P. Tzanetakis, S. H. Anastasiadis, C. Fotakis, *Adv. Mater*., 2008, **20**, 4049.

28 B. D. Choudhury, A. Abedin, A. Dev, R. Sanatinia, S. Anand, *Opt. Mater. Express*, 2013, **3**, 1039.

29 B. Hua, B. Wang, M. Yu, P. W. Leu, Z. Fan, *Nano Energy*, 2013, **2**, 951.

30 Z. Fan, R. Kapadia, P. W. Leu, X. Zhang, Y. L. Chueh, K. Takei, K. Yu, A. Jamshidi, A. A. Rathore, D. J. Ruebusch, M. Wu, A. Javey, *Nano Lett*., 2010, **10**, 3823.

31 J. Shieh, F. J. Hou, Y. C. Chen, H. M. Chen, S. P. Yang, C. C. Cheng, H. L. Chen, *Adv. Mater*., 2010, **22**, 597.

32 J. Shieh, S. Ravipati, F. H. Ko, K. K. Ostrikov, *J. Phys. D*, 2011, **44**, 174010.

33 S. Kurtin, G. A. Shifrin, T. C. McGill, *Appl. Phys. Lett*., 1969, **14**, 223.

34 C. H. Lin, H. L. Chen, W. C. Chao, C. I. Hsieh, and W. H. Chang, *Microelectron. Eng.*, 2006, **83**, 1798.

35 K. Watanabe, *J. Opt. Soc. Am. A*, 2002, **19**, 2245.